Neuropilin-2 upregulation by stromal TGFβ1 induces lung disseminated tumour cells dormancy escape and promotes metastasis outgrowth

Leire Recalde-Percaz
Barcelona University
Patricia Jauregui
Navarra University
Anna López-Plana
Barcelona University
Patricia Fernandéz-Nogueira
Barcelona University
Minerva Iniesta-González
Complutense University
Sara Manzano
Biodonostia
Raul Alonso
Barcelona University
Aleix Noguera-Castells
Barcelona University
Nuria Moragas
Barcelona University
Cristina Baquero
Complutense University
Maria Rodrigo-Faus
Complutense University
Nerea Palao
Complutense University
Erica Dalla
Icahn School of Medicine at Mount Sinai
Francesc Xavier Aviles-Jurado
Hospital Universitari Joan XXIII de Tarragona
Isabel Vilaseca
Hospital Clinic
Mercedes Camacho

Sant Pau Hospital
Xavier Leon-Vintro
Sant Pau Hospital
Gemma Fuster
Vic University
Jordi Alcaraz
University of Barcelona https://orcid.org/0000-0001-7898-1599
Julio Aguirre-Ghiso
Albert Einstein College of Medicine https://orcid.org/0000-0002-6694-6507
Pere Gascón
Barcelona University
Álvaro Gutierrez-Uzquiza
Department of Biochemistry and Molecular Biology, Faculty of Pharmacy, Complutense University Madrid, Spain
Almudena Porras
Department of Biochemistry and Molecular Biology, Faculty of Pharmacy, Complutense University Madrid, Spain https://orcid.org/0000-0002-6495-3308
Neus Carbo
Barcelona University
Paloma Bragado (pbragado@ucm.es)
Department of Biochemistry and Molecular Biology, Faculty of Pharmacy, Complutense University of Madrid

---

Article

Keywords: Neuropilins, dormancy, disseminated tumour cells, TGFβ, metastasis, breast cancer, head and neck cancer

Posted Date: August 15th, 2022

DOI: https://doi.org/10.21203/rs.3.rs-1956933/v1

Neuropilin-2 upregulation by stromal TGFβ1 induces lung disseminated tumour cells dormancy escape and promotes metastasis outgrowth

Recalde-Percaz L[1,2], Jauregui P[1], Lopez-Plana A[1,2], Fernández-Nogueira P[1,2], Iniesta-González M[3], Manzano S[3,4,5], Alonso R[1], Noguera-Castells A[1,2], Moragas N[1,2], Baquero C[3,4], Rodrigo-Faus M[3,4], Palao N[3,4], Dalla E[6], Avilés-Jurado FX[7,8], Vilaseca I[9,10,11], León-Vintró X[12,13], Mercedes Camacho[14], Fuster G[1,2,15], Alcaraz J[16,17], Aguirre-Ghiso J[6,18], Gascón P[1,2], Gutiérrez-Uzquiza, A[3,4], Porras A[3,4], Carbó N[2], Bragado P[3,4]

[1]Department of Biomedicine, School of Medicine, University of Barcelona, 08028 Barcelona, Spain
[2]Department of Biochemistry and Molecular Biomedicine, Faculty of Biology, Institute of Biomedicine of the University of Barcelona (IBUB), 08028, Barcelona, Spain
[3]Department of Biochemistry and Molecular Biology, Faculty of Pharmacy, Complutense University of Madrid, 28040 Madrid, Spain
[4] Health Research Institute of the Hospital Clínico San Carlos, 28040 Madrid, Spain.
[5] Instituto de Investigación Sanitaria (IIS) Biodonostia, 20014 San Sebastián/Donosti, Spain
[6]Department of Cell Biology, Cancer Dormancy and Tumor Microenvironment Institute, Albert Einstein Cancer Center, Albert Einstein College of Medicine, New York, NY, USA.
[7]IISPV, Institut d'Investigació Sanitària Pere Virgili, 43002 Tarragona, Spain.
[8]Head Neck Section, Otorhinolaryngology Department, Hospital Universitari Joan XXIII de Tarragona, 43005 Tarragona, Spain.
[9] Functional Unit of Head and Neck Tumors. Otorhinolaryngology Head-Neck Surgery Department, Hospital Clínic, Barcelona, Spain.
[10]Translational Genomics and Target Therapies in Solid Tumors Group. Institut d´Investigacions Biomèdiques August Pi i Sunyer. IDIBAPS. Barcelona. Spain
[11]Surgery and Medical-Surgical Specialties Department. Faculty of Medicine and Health Sciences. Universitat de Barcelona. Barcelona. Spain.
[12]Otorhinolaryngology Department, Hospital de la Santa Creu i Sant Pau, Universitat Autònoma de Barcelona, 08193 Barcelona, Spain.
[13]Centro de Investigación Biomédica en Red de Bioingeniería, Biomateriales y Nanomedicina (CIBER-BBN), 28001 Madrid, Spain.
[14]Genomics of Complex Diseases, Research Institute Hospital Sant Pau, IIB Sant Pau, 08041 Barcelona, Spain
[15]Department of Biosciences, Faculty of Sciences and Technology, University of Vic, 08500 Vic, Spain
[16]Unit of Biophysics and Bioengineering, Department of Biomedicine, School of Medicine and Health Sciences, Universitat de Barcelona, Barcelona, Spain
[17]Institute for Bioengineering of Catalonia (IBEC), The Barcelona Institute for Science and Technology (BIST), Barcelona 08028, Spain.
[18]Gruss-Lipper Biophotonics Center, Ruth L. and David S. Gottesman Institute for Stem Cell Research and Regenerative Medicine Albert Einstein Cancer Center, Albert Einstein College of Medicine, New York, NY, USA.

Correspondence to: Paloma Bragado (pbragado@ucm.es)

Running title: *Neuropilin-2 promotes lung metastasis*

Key words: Neuropilins, dormancy, disseminated tumour cells, TGFβ, metastasis, breast cancer, head and neck cancer

ABSTRACT

Metastasis is the main cause of death from solid tumours and, therefore, identifying the mechanisms that govern metastatic growth poses a major biomedical challenge. We and others have contributed to demonstrate that tumour microenvironment (TME) signals regulate the fate and survival of disseminated tumour cells (DTCs) in secondary organs. However, very little is known about the role of the nervous system mediators in this process. We have previously described that neuropilin-2 (NRP2) expression in breast cancer correlates with bad prognosis. Here we describe that NRP2 positively regulates breast and head and neck cancer cells proliferation, invasion and survival *in vitro*. NRP2 deletion in tumour cells inhibits tumour growth *in vivo* and decreases the number and size of lung metastases by promoting p27-mediated lung DTCs quiescence. Moreover, we show that several abundant stromal cells of the lung, such as fibroblasts and macrophages, induce NRP2 upregulation in DTCs, through secretion of TGFβ1. Therefore, we conclude that the TGFβ1-NRP2 axis is a new key dormancy awakening inducer, promoting DTCs proliferation and lung metastases development, positioning NRP2 expression as a central biomarker to predict metastatic recurrences and as a potential candidate for advanced therapies.

INTRODUCTION

Metastasis is the dissemination of tumour cells to a secondary organ where a macroscopic secondary tumour will grow. It is the main cause of death associated to solid tumours since more than 90% of patients will die from metastatic diseases[1]. Metastasis is considered the last of a complex and dynamic cascade of steps in which tumour cells grow, escape from the primary tumour (PT), migrate, intravasate, disseminate via the circulatory system, colonize secondary organs, enter dormancy, survive, and finally reinitiate growth to form secondary tumours[1,2]. Metastases derive from DTCs that escape from the primary tumour (PT) and invade secondary organs, where they proliferate generating a secondary tumour bulk[2,3]. However, metastases can appear months or years after PT diagnosis and treatment due to a clinically occult state that DTCs acquire, known as dormancy, in which they become quiescent and resistant to anti-proliferative therapies[3,4]. Dormancy is a reversible cell cycle arrest from which DTCs can escape through mechanisms that remain unclear[2].

According to the seed and soil theory (S. Paget, 1889)[5,6], the TME exerts a regulatory effect on the biology of metastases and DTCs, tightly controlling metastases development. In agreement with this, we previously showed that in head and neck squamous cell carcinoma (HNSCC) models, TGFβ2, regulates DTCs quiescence in the bone marrow (BM) through binding to TGFβR3[7]. Likewise, other studies have reported additional TME regulators of DTCs fate such as TSP-1[8], Gas6[9] or BMP7[10]. However, the mechanisms that control DTCs dormancy, re-activation and proliferation are still not well understood.

In recent years, the contribution of nerves and neural derived factors to the regulation of tumour progression has emerged as an important component of the TME[11,12]. Two pioneer studies in prostate[13] and gastric cancer[14] showed that nerves are an essential component of the TME and that neoneurogenesis plays a key role in cancer progression and metastasis. More recently, it was shown that the remodelling of the extracellular matrix by schwann cells potentiates metastasis initiation[15]. Furthermore, it also has been reported that the sympathetic nervous system is also implicated in the reactivation of dormant DTCs in the BM niche[16]. Using bioinformatics tools and patient databases we identified several neuronal related genes that are differentially expressed among breast cancer (BrCa) subtypes[17], suggesting that neural-related factors are implicated in BrCa initiation and progression. Neuropilin-2 (NRP2) appeared to be over-expressed in the basal-like BrCa subtype[17], the most aggressive BrCa subtype that usually presents low dormancy periods and develops metastasis in the first 5 years after diagnosis.

Furthermore, high NRP2 expression in triple negative BrCa patients correlated with worse prognosis[17]. Similarly, in HNSCC, transcriptional expression of Semaphorin-3F and NRP-2 correlates with a higher risk of occult nodal metastases[18]. NRPs are multifunctional proteins that act as co-receptors for class 3 semaphorins (SEMA3s) and for diverse growth factor molecules such as vascular endothelial growth factors (VEGF) and TGFβ1[19]. NRPs expression is commonly aberrant in tumours and thus, they can modulate multiple tumorigenic processes[20]. How DTCs interact with neural-derived cues present in the microenvironment to regulate dormancy and survival in metastatic sites is largely unknown. In this study we have defined the role of NRP2 in DTCs regulation and progression into metastasis in preclinical models of BrCa and HNSCC.

METHODS

Cells lines and cultures

Human BrCa cell lines were obtained from the American Type Culture Collection (ATCC; Rockville, MD) and grown in DMEM, DMEM/F12 or RPMI-1640 media at 37ºC and 5% CO_2 according to the ATCC indications for each cell line. Media was supplemented with 10% foetal bovine serum (FBS), 5% Glutamax and 5% Penicillin-Streptomycin (Gibco), hereafter referred to as complete culture media. In the case of BT-549 and BT-474 cell lines media were supplemented with 10µg/mL of human insulin (Sigma-Aldrich). MDA-MB-453-PT and MDA-MB-453-Lu cell lines were obtained and cultured as previously published[21].

HNSCC cell lines were generated as previously described[7] and grown in DMEM/F12 complete media at 37ºC and 5% CO_2. HEp3 cells were maintained as primary cultures and cultured *in vitro* up to passage 4. They were maintained *in vivo* using the chicken embryo chorioallantoic membrane (CAM)[22] or nude mice systems.

The human lung fibroblasts CCD-19Lu cells were kindly donated by Dr. Alcaraz (University of Barcelona, Spain) and cultured in DMEM/F12 complete media at 37ºC and in 5% CO_2. The human monocyte cell line THP-1 was kindly donated by Dr. Julve (University of Barcelona, Spain). THP-1 cells were cultured at 37ºC and 5% CO_2 according to the ATCC indications. They were differentiated into monocyte-derived macrophages using 50ng/mL of 12-O-tetradecanoylphorbol-l3-acetate (PMA; Sigma-Aldrich) for 4 days. Total differentiation of monocyte-derived macrophages was obtained by removing the PMA containing media and incubating the cells in fresh culture media for 1-2 days.

Generation of conditioned media

For the experiments with conditioned media (CM), cell lines were cultured up to 80% confluence and maintained in serum-free media for 48h. Their culture media was collected, filtered with 0.22µm filters and centrifuged (1200rpm, 5min) to discard unattached cells and cell debris. For lung CM generation, lung tissues from healthy animals were dissected and dissociated by incubation with 200U/mL collagenase type IV and 100U/mL bovine serum albumin (BSA) solution (#C9891, Sigma-Aldrich) for 30min at 37ºC. The tissue cell suspension was homogenized, centrifuged and the cell pellet was resuspended in DMEM/F12 complete media. After 24h, fresh cell media was added and when 80% confluence was obtained, lung CM was generated as previously described[7].

CRISPR/Cas9

To efficiently delete NRP2, the CRISPR-Cas9 technology using the double lentiviral system designed by Zhang laboratory, was used[23] (check further details in supplementary Materials and Methods). First, Cas9-expressing T-HEp3 and MDA-MB-231 cells were developed. Then, specific NRP2 guide RNAs (gRNA) were annealed and cloned in lentiGuide-puro (LG) plasmid (#52963, Addgene) using BsmBI cloning site (5'-CACCGGACTGCAAGTACGATTGGC-3' (forward) and 5'-AAACGCCAATCGTACTTGCAGTCC-3' (reverse)). Finally, Cas9 expressing T-HEp3 and MDA-MB-231 cells were infected with non-targeting control (NTC) or NRP2 gRNA carrying lentiviruses. After 24h, media was changed and 48h later, blasticidin (10µg/mL) and puromycin (1µg/mL) selection was performed. Single cell clones were expanded and NRP2 deletion was verified by qPCR and western blot.

Immunoprecipitation assay

To deplete TGFβ1 from CM, 10mg/mL magnetic beads (#10003, Invitrogen) were incubated with 10µg anti-TGFβ1 antibody (#sc-52893, Santa Cruz) or matched IgG isotype control (#31903, Invitrogen) in serum-free media. The beads-antibody solution was pre-incubated during 1h at 4ºC and rotation movement. The magnetics beads were isolated using the magnetic rack and 1mL of the CM was added and incubated overnight (ON) at 4ºC with rotation movement. The next day, centrifugation and isolation of magnetic beads was performed using the magnetic rack and the supernatant was collected for its immediately use for cell treatment.

Cell cycle assay

To determine the effect of NRP2 deletion on the cell cycle, cells were seeded and grown until 70-80% confluence. Then, serum deprivation was performed for 24h. Cells were

fixed with cold 70% ethanol added dropwise in slight rotational movement. Fixed cells were incubated for 15min at 4ºC with propidium iodide/RNase Staining Buffer (#550825, BD Pharmingen) adding 500µL of the buffer for every 10^6 cells. Finally, cells were resuspended in PBS and analysed using flow cytometry (Fortessa LSR) and quantified using FACSDIVA software (BDBiosciences). 10,000 cells were analysed for each sample and duplicates were performed for each experimental condition.

3-(4,5-Dimethylthiazol-2-yl)-2,5-diphenyltetrazolium bromide (MTT) assay

To analyse *in vitro* cell proliferation and viability, a 4-days based MTT assay was performed using the Cell Titer 96 Aqueous One Solution Cell Proliferation Assay Kit (#G3581, Promega). Briefly, 7000 cells were seeded in a final volume of 200µL per well in MW96 plates. Cells were cultured in 2% FBS containing media. After 24h, the colorimetric assay was performed by removing 80µL of media from each well and adding 20µL of the tetrazole MTT reagent. This process was also performed in three wells with no cells where only culture media was added for developing the blank measurements. After 1.5h incubation at 37ºC, absorbance at 492nm and 620nm was measured. This procedure was repeated every day during 4 days in a row, with 6 replicates for each condition.

Colony formation assay

For measuring the anchorage-dependent growth ability, 300 cells were seeded in 60mm diameter dishes in 5% FBS culture media. Cell media was changed every 2-3 days and cells were grown at 37ºC and 5% CO_2 for 1-3 weeks until independent colonies were formed. Then, cells were fixed and stained with crystal violet (HT90132; Sigma-Aldrich). Colonies area and number were quantified using ImageJ software. Experiments were performed in triplicate.

Wound-healing assay

Cells were seeded in 24-well tissue culture plates so that at 24h they reach 70-80% confluence as a monolayer. Confluent monolayers were scratched using a plastic pipette tip to draw a linear wound. The medium was then replaced with fresh serum-free medium and the required treatment, when necessary. Cells were allowed to migrate for 24-48h or until the wound was closed, at 37ºC and 5% CO_2. Cell migration was followed over time by a phase-contrast LEICA DFC295/DMIL LED microscope coupled to a digital camera. Photos were taken at different time points (0h, 4h, 8h and 24h) and the migration capacity of the cells was determined quantifying the percentage of the wound closing area using the ImageJ software.

Transwell invasion assay

An extracellular matrix layer was generated in 6.5mm Transwell® with 8.0µm pore polycarbonate membrane inserts (#3422, Corning) using BD Matrigel™ Basement Membrane Matrix (#354234, Biosciences) in a 1:9 ratio with serum-free media. $1 \cdot 10^5$ cells were seeded on top of the matrigel layer in serum-free media. FBS-containing complete culture media was used in the lower chamber as a chemoattractant. After 24h, invading cells were fixed with 4% paraformaldehyde (PFA) and stained with crystal violet for 30min at room temperature (RT). The inserts were air-dried before taking photos by a digital camera coupled to a phase-contrast microscope for cell counting.

***In vivo* mice models**

All animal experiments were performed in accordance with our institution's ethics commission's regulations, following the guidelines established by the regional authorities (Catalonia, Spain). Five-week-old female NOD-SCID mice (CB17/IcrHanHsd-PrKdc Scid) were obtained from Janvier Labs (France, Europe) and kept under specific-pathogen free (SPF) health conditions at constant ambient temperature (22–24°C) and humidity (30–50%). The MMTV–Her2 immune-competent transgenic mice were bred in and obtained from the Aguirre-Ghiso's laboratory at Mount Sinai School of Medicine, USA. 14 to 18-weeks-old female mice were used as early ('pre-malignant') stage and 20-weeks-old female mice with palpable tumour(s) were used as late stage of cancer progression[24]. For the fibrosis experiments, we used Rapgef1$^{Flox/Flox}$; PF4-Cre$^{-/-}$ mice that were bred in and obtained from Dr. Porras' laboratory at Complutense University, Spain. Young (6-weeks mice) 'mice' and old (16-month-old) months mice were used.

Xenograft tumours were obtained by orthotopic inoculation of 1:1 ratio mixture of matrigel and PBS++ (supplemented with 1mM $MgCl_2$ and 0.5mM $CaCl_2$), in a final volume of 100µL per mouse. Either $8 \cdot 10^5$ of T-HEp3-NTC or T-HEp3-NRP2^{KO} cells were inoculated in mice neck area (5 mice per condition). 10^6 MDA-MB-453 cells were inoculated in the mammary gland. Mice weight and tumour size were measured twice per week using a calliper, where tumour volume (V) was calculated as $V=(D*d)^2/2$ (D: long diameter; d: short diameter). In the MDA-MB-453 model, mice were euthanized after 3 months. For the T-HEp3 model, once tumour volumes mean were over 500mm^3, PTs were surgically removed, and mice were left for an additional 4 weeks period. Surgically removed PTs were measured, weighted, and stored at -80ºC for protein and RNA extraction or fixed in 4% PFA for further immunohistochemical analyses. After 4 weeks growth, mice were anesthetized and euthanized in accordance with the regulations of the institution's ethics

commission. At the end point, potential metastatic organs such as the lungs were surgically removed and fixed in 4% PFA for the analysis of the presence of DTCs.

For the lung metastasis *in vivo* experiments, $2.5 \cdot 10^5$ of wild-type T-HEp3, T-HEp3-NTC or T-HEp3-NRP2^{KO} cells or $5 \cdot 10^5$ of MDA-MB-231-Cas9 or MDA-MB-231-NRP2^{KO} cells were inoculated in a final volume of 100µL in PBS++ into the lateral caudal tail vein (5 mice per group). Mice weight was measured twice per week. 2 and 4 weeks after inoculation, mice were anesthetized and euthanized in accordance with the regulations of the institution's ethics commission. At the end point, lungs were removed for metastasis assessment, by fixing them in 4% PFA for the analysis of the presence of DTCs by immunocytochemistry.

Studies with patients

NRP2 mRNA expression was analysed using BrCa patients' data from GOBO[25] and Kaplan-Meier plotter[26] public databases. In addition, in collaboration with Dra. Camacho and Dr. Leon from Sant Pau Hospital (Barcelona, Spain), *NRP2* mRNA expression was analysed by RT-qPCR in PT samples from a cohort of 92 HNSCC patients and correlated with distant metastasis-free survival (DMFS).

Statistical analyses

The results were graphically plotted and statistically analysed using GraphPad Prism7 software. Graphs represent the mean value of the samples ± standard error of the mean (S.E.M.). To compare two experimental groups, the unpaired *t*-Student's test was used whereas one-way ANOVA or two-way ANOVA tests were used to compare more than two groups, with one or two variables, respectively. Multiple comparison tests were performed afterwards. Statistical significance was considered when the p-value was lower than 0.05, following the next annotation: *p-value ≤ 0.05, **p-value ≤ 0.01, ***p-value ≤ 0.001 and ****p-value ≤ 0.0001.

RESULTS

NRP2 promotes proliferation and cell cycle progression concomitantly with p27 inhibition

To determine the role of NRP2 in dormancy regulation, we first assessed the expression of NRPs in a panel of BrCa cells previously characterized as either proliferative/low-dormancy score (LDS) or dormant-like/high-dormancy score (HDS) cells[27] based on the ratio between the expression of positive dormancy genes and negative dormancy genes which identified MDA-MB-231, MDA-MB-468, HCC1954 and BT-549 as LDS cell lines

and BT-474, T-47D, MDA-MB-453 and ZR-75-1 as HDS cells[27]. We observed that *NRP1* and *NRP2* mRNA were up-regulated in LDS cell lines compared to HDS cells, whereas *NRP2* gene expression was down-regulated in HDS cells compared to non-malignant mammary epithelial MCF10A cells (**fig. 1A**). Consistently, NRP2 protein expression was up-regulated in LDS cells, particularly in MDA-MB-231 and BT-549, whereas it was poorly expressed in HDS cell lines (**fig. 1B**). We also examined the expression of NRPs in a panel of HNSCC cell lines with a known proliferative or dormant phenotype previously generated from lungs (Lu) or bone marrow (BM) DTCs using a HNSCC patient derived xenograft (PDX) model (T-HEp3)[7]. The lung DTCs derived cells (Lu-HEp3) are proliferative/LDS, whereas the BM DTCs derived cell line (BM-HEp3) exhibits a quiescent/dormant/HDS phenotype[7]. In addition, we used an *in vitro* derived dormant variant of HEp3 (D-HEp3)[7,28]. Analysis of NRPs mRNA and protein expression in HNSCC cells confirmed that NRP1 and NRP2 were up-regulated in proliferative/LDS cells, not only in the parental cell line, but also in the cell line derived from Lung DTCs (**fig. 1C, D**). NRP1 expression was also downregulated in BrCa and HNSCC HDS cell lines (**Supplementary Fig. 1A-B)**. However, Lu-Hep3 cell express very low levels of NRP1 both at the mRNA and protein levels (**Supplementary Fig. 1C-D).** These results reveal that NRP2 expression is down-regulated in both BrCa and HNSCC dormant cells lines whereas its expression correlates with a more proliferative phenotype and is upregulated in the lung DTCs derived cell line.

Prompted by our observed inverse correlation between NRP2 expression and quiescence, we sought to characterize NRP2 role in cell proliferation by generating stable NRP2-knockouts ($NRP2^{KO}$) in LDS cell lines from BrCa and HNSCC through CRISPR-Cas9 (**Supplementary Fig. 1E-G**). We first analysed NRP2 role in tumour cells proliferation and found that$NRP2^{KO}$ cells proliferated more slowly than control cells, both in MDA-MB-231 (**fig. 1E**) and T-HEp3 cells (**fig. 1F**). Furthermore, we found that NRP2 deletion induces cell cycle arrest (**fig. 1G-H**). MDA-MB-231 $NRP2^{KO}$ cells were arrested in G2/M phase (**fig. 1G**) while T-HEp3 $NRP2^{KO}$ cells were arrested in G1 (**fig. 1H**). Cell cycle progression relies on protein complexes composed by cyclins and cyclin dependant kinases (CDKs). To prevent abnormal proliferation, nuclear Cip/Kip proteins, such as p21 and p27, act as catalytic inhibitors of CDKs[29]. Analysis of p27 expression showed that NRP2 expression modulation either by inhibiting its activity using a NRP2 blocking antibody (αNRP2), silencing its expression using siRNA against NRP2 or by the complete deletion of NRP2 notably increased p27 protein levels (**fig. 1I-K**). However, no significant differences were observed in standard dormancy markers other than p27, including the levels of phosphorylated (active) p38 MAPK and ERK, and the p-ERK/p-

p38 ratio[7,30] (**Supplementary Fig. 1H-I**), suggesting that other factors altered upon NPR2 loss may be required to elicit a full dormant phenotype. Collectively, these results indicate that NRP2 is a pro-tumorigenic and/or anti-dormancy protein, that induces cell proliferation while inhibiting cell cycle arrest, probably through reducing p27 levels.

NRP2 deletion inhibits tumour-initiation capacity *in vitro* and blocks tumour growth *in vivo*

To test whether NRP2 could also regulate tumour-initiation capacity, we performed anchorage dependent colony formation assays and observed that NRP2 deletion decreased the number of foci formed by MDA-MB-231 cells (**fig. 2A**) and T-HEp3 cells (**fig. 2B**), unraveling the tumour-initiation capacity enhancement of NRP2 in BrCa and HNSCC cells.

We then analysed the specific contribution of NRP2 to tumour growth *in vivo* by orthotopically inoculating NRP2 knockout and control T-HEp3 cells. When PTs reached volumes over 500mm^3, they were surgically removed (**fig. 2C**). NRP2 depletion strongly suppressed tumour growth *in vivo*, whereas control tumours derived from NTC cells grew vigorously. In fact, control tumours had to be surgically removed 16 days after inoculation (**fig. 2D**). Interestingly, NRP2^{KO} cells derived tumours had a delay of 1 month in growth in comparison with the control group, further supporting its role as a dormancy-regulatory protein (**fig. 2D**). Moreover, NTC tumours were bigger than NRP2^{KO} tumours regarding PTs weight and volume (**fig. 2E**), corroborating that NRP2 has a key role in promoting tumour growth *in vivo*. NRP2 expression remained low in tumours bearing NRP2^{KO} cells (**fig. 2F**) and, in agreement with the *in vitro* experiments, deletion of NRP2 increased p27 levels in tumour samples as well, although this difference did not reach statistical significance (**fig. 2G**). Additionally, NRP2 depletion increased the expression of the apoptotic marker cleaved caspase 3 (cc3) in NRP2^{KO} cells derived tumours (**fig. 2H**) suggesting NRP2 could also be promoting tumour cells survival. Altogether, these results suggest that NRP2 deletion reduces HNSCC tumour growth *in vivo* by promoting quiescence and apoptosis.

NRP2 upregulation in lung DTCs drives lung micro-metastases emergence

Once identified the link between NRP2 expression and cancer cell proliferation and tumour growth *in vitro* and *in vivo*, we characterized the role of NRP2 in migration and invasion *in vitro*. Wound-healing assays revealed that NRP2^{KO} MDA-MB-231 cells migrate less than Cas9 control cells (**fig. 3A**), whereas NRP2 deletion in T-HEp3 cells had no effect on cell migration capacity (**Supplementary Fig. 2**), suggesting that the

NRP2 role in regulating cell migration may be cell type dependent. In contrast, the invasion capacity of the NRP2-depleted cells was significantly reduced as compared to control in both MDA-MB-231 (**fig. 3B**) and T-HEp3 (**fig. 3C**) cells, revealing that NRP2 promotes cancer cell invasion, which is a major step towards increased dissemination.

Our observation that NRP2 is upregulated in proliferative compared to dormant cells lines and that this overexpression promotes tumour growth, colony formation and invasion provides new insights on the role of NPR2 in the context of the primary tumour. Next, we wondered whether NRP2 may also regulate DTCs shift between proliferation and quiescence in colonized organs. For this purpose, we first examined NRP2 expression in lung DTCs *in vivo* in xenograft models. We stained chicken and mice lungs from control animals in order to detect T-HEp3 lung DTCs by vimentin-positive staining (**fig. 3D**, top and middle panel). We also used the MMTV-Neu mice model for BrCa where multifocal breast carcinomas with lung metastases are developed after 12-16 weeks of growth[31] to detect BrCa lung DTCs (by HER2 staining) (**fig. 3D**, bottom panel). We found that vimentin in T-HEp3 DTCs and HER2 in BrCa DTCs were co-expressed with NRP2 (**fig. 3D**), revealing that NRP2 is expressed in PTs-derived lung DTCs. Moreover, in a lung metastasis *in vivo* experiment with wild-type T-HEp3 cells we observed that the number of NRP2-positive cells was statistically significantly higher in late lung macrometastases (isolated 3 weeks after inoculation) as compared to early lungs (isolated 1 week after inoculation) (**fig. 3E**). Finally, to test if NRP2 expression in lung DTCs could be regulated by the lung microenvironment, we inoculated MDA-MB-453 cells (low tumorigenic, HDS and low expression of NRP2) orthotopically into mice mammary fat pad and let tumours grow for a long period (12 weeks)[21]. At end point, lungs were isolated and cell dissemination was analysed by detecting lung DTCs by HER2 staining. Surprisingly, we found that while single DTCs were still negative or express very low levels of NRP2 (**fig. 3F**, upper panel), MDA-MB-453 DTCs-derived lung micrometastases upregulated NRP2 (**fig. 3F**, lower panel). These findings were validated in PTs and lung DTCs (Lu) derived MDA-MB-453 primary cell lines analysis, which showed increased expression of NRP2 in the cell lines derived from lung DTCs (**Supplementary Fig. 3**). This suggests that up-regulation of NRP2 optimizes DTC conversion from a solitary cell state to proliferative clusters and metastasis outgrowth and support that the lung microenvironment can up-regulate NRP2 expression.

To delve into the role of NRP2 in lung DTCs, we used the lung DTCs primary cell line Lu-HEp3 which over-expresses NRP2 (**fig. 1D**). Treatment of Lu-HEp3 cells with a NRP2 blocking antibody (αNRP2) *in vivo* had no effect on Lu-HEp3 PTs size (**Supplementary Fig. 4A**), although the levels of the proliferation marker Ki67 decreased in the tumours

treated with the NRP2 blocking antibody *in vivo* (**Supplementary Fig. 4B**), suggesting that blocking NRP2 decreases Lu-HEp3 cells proliferation. In addition, blocking NRP2 activity increased the apoptotic marker cc3 levels in Lu-HEp3 tumours (**Supplementary Fig. 4C**), relating NRP2 to lung DTCs survival too. Consequently, these results highlight the key role of NRP2 in the regulation of lung DTCs growth and survival.

Lung fibroblasts and macrophages derived TGFβ1 induces DTCs NRP2 expression

We next explored the mechanisms that may support NRP2 up-regulation in lung microenvironment that might favour metastasis. It has been reported that NRPs act as co-receptors of several soluble ligands and can be regulated by factors present in the TME[19,32,33], such as VEGF. We first treated the cells with VEGF-C, the main vasculogenic ligand of NRP2 to induce lymphatic endothelial cells proliferation and favouring cell migration and invasion[34]. Surprisingly, no differences in NRP2 levels were observed (**Supplementary Fig. 5A**). No effects were either observed when cells were treated with SEMA3F, the most important ligand of NRP2 regulating axonal guidance in the nervous system[35] and tumour cell dissemination[36] (**Supplementary Fig. 5B**).

In contrast treatment of proliferative BrCa and HNSCC cells with TGFβ1, which has been shown to promote DTCs proliferation[7], induced a clear up-regulation of NRP2 protein levels (**fig. 4A and Supplementary Fig. 5C**). Notably, NRP2 levels returned to the basal levels both in BrCa and in HNSCC cell lines when treated with type I TGFβ receptor inhibitor SB431542, implicating the TGFβ1 canonical pathway in NRP2 overexpression (**fig. 4A**). Furthermore, TGFβ1 treated 3D-cultured cells showed bigger colony formation and higher NRP2 and Ki67 expression (**Supplementary Fig. 5D, E**), further confirming the link between NRP2 expression and proliferation.

These results suggest that the lung microenvironment could promote NRP2 expression. To test this hypothesis, we collected lung conditioned media (CM) from healthy mice lungs and use it to stimulate both BrCa and HNSCC proliferative cells. After 24h, we found that NRP2 was highly up-regulated in lung CM treated cells, whereas this effect was partially reverted when type I TGFβ receptor was inhibited (**fig. 4B**).

Next, we checked TGFβ1 levels in lung CM (**fig. 4C**). As expected, we found that the lung CM is rich in TGFβ1 compared to normal media or MDA-MB-231 and T-HEp3 media (**fig. 4C**). To confirm that the lung CM upregulation of NRP2 was dependent on TGFβ1, we repeated these experiments using lung CM with a partial TGFβ1 depletion (αTGFβ1 lung CM) (**fig. 4D**). The NRP2 up-regulation derived from the non-depleted lung CM was partially abrogated in T-HEp3 cells when TGFβ1 was reduced from the lung CM (**fig.**

4E). Altogether, these results strongly suggest that lung-derived TGFβ1 could be a major factor up-regulating NRP2 expression in lung DTCs.

Macrophages and fibroblasts have been pointed as critical tumour-growth promoting stromal cells in the lung[37,38] and major producers of TGFβ1 within the lung microenvironment[38]. We first verified that (THP-1-derived macrophages and CCD19 lung fibroblasts synthetized and released TGFβ1 to the media at higher levels than tumour cells (**fig. 4F**). Then, we collected macrophage and fibroblasts condition media and treated our cells with it. In response to stimulation with THP-1 macrophages CM (THP-1 CM), we found that NRP2 expression was markedly increased (**fig. 4G**), not only in BrCa and HNSCC proliferative cells but also in HNSCC lung DTCs (Lu-HEp3) (**fig. 4G**). Likewise, CCD19-Lu lung fibroblasts CM (CCD19 CM) induced NRP2 overexpression (**fig. 4H**). Conversely, inhibition of the TGFβ canonical pathway with the type 1 TGFβ receptor was sufficient to abrogate NRP2 overexpression in all settings, (**fig. 4G, H**). indicating that lung fibroblasts and macrophages secrete TGFβ1 which will increase NRP2 expression in tumour cells that already express NRP2 through a mechanism involving the TGFβ canonical pathway.

It has been described that TGFβ1-driven lung fibrosis promotes dormant lung DTCs re-awakening and generation of overt lung metastases[39]. Therefore, we wondered whether lung fibrosis-induced cancer cell proliferation could be regulated by NRP2. Using young (6 weeks) and old (16 months) mice, we prepared lung CMs and analysed if there were differences in NRP2 protein levels in T-HEp3 cells upon treatment with these CMs. Higher expression of the activated fibroblasts marker αSMA (α-smooth muscle actin) in old lungs corroborated that they were more fibrotic (**fig. 4I**). Consistently, old lungs had higher levels of TGFβ1 (**fig. 4J**). When we treated cancer cells with these CMs, both young and old lungs CM treatments up-regulated NRP2 (**fig. 4K**). Interestingly, SB431542 treatment reverted NRP2 induction by the old lung CM, while had little effect on NRP2 induction by young lung CM (**fig. 4K**). These results indicated that TGFβ1 regulation of NRP2 induction might be age-dependent, so that TGFβ1, that is more abundant in fibrotic old lungs, could be associated both with NRP2 up-regulation and dormant lung DTCs re-awakening. It also raises a question on the relevant contributions of other stromal signals, besides TGFβ1, which contribute to DTCs awakening in younger lungs.

NRP2 deletion triggers quiescence in lung DTCs *in vivo and inhibits* lung metastases

Our previous results have shown that NRP2 is up-regulated in lung DTCs and it promotes cell proliferation while inhibiting the dormancy marker p27. To further uncover the pathologic role of NRP2 on lung DTCs biology, we let the tumours grow for 28 days or until they reached 500mm^2 in the T-HEp3 xenograft model, performed PTs surgery and kept mice for 4 weeks and isolated lung DTCs (**fig. 5A**). Lung DTCs were identified by human vimentin expression (as a mesenchymal tumour cell marker) and their phenotype was determined by the proliferation marker Ki67 signal (Ki67-positive, proliferative DTC; Ki67-negative, dormant DTC). We found that lung micrometastases developed from NRP2^{KO} cells were significantly smaller than the controls (**fig. 5B**). Moreover, NRP2 deletion significatively increased the percentage of dormant single lung DTCs (**fig. 5C**).

To rule out that these effects were caused by defects in NRP2^{KO} cells dissemination, invasion or colonization of secondary organs, as suggested by our observation that NRP2^{KO} cancer cells are less invasive (Fig 3B-C), we performed a tail vein *in vivo* experiment by inoculating MDA-MB-231 or T-HEp3 control (Cas9/NTC) or NRP2^{KO} cells. Lungs were isolated 2 and 4 weeks post-inoculation, and cell dissemination was examined (**fig. 5D**). In the BrCa model, NRP2^{KO} macrometastases (4 weeks) were significantly smaller than Cas9 macrometastases (**fig. 5E**). Moreover, NRP2^{KO} derived DTCs displayed a more dormant phenotype, a prominent effect clearly observed in doublet lung DTCs (**fig. 5F**). In the HNSCC model, no macrometastases were found 2 weeks after the inoculation (data not shown), while the number of single and double dormant DTCs clearly increased in NRP2^{KO} injected mice at 2 weeks (**fig. 5G**). These effects were also evidenced after 4 weeks, when a significant reduction in the size of macrometastases was found in NRP2^{KO} mice (**fig. 5H**). The number of dormant single and double lung DTCs derived from NRP2^{KO} cells was also significantly increased (**fig. 5I**). These results underscore that NRP2 exerts an important function in lung metastases development by inhibiting lung DTCs dormancy and promoting the proliferative phenotype of DTCs, thereby favouring the development and enlargement of lung metastases.

High levels of NRP2 negatively correlate with BrCa and HNSCC patients' distant metastases free survival

The initial characterization of NRPs expression unveiled the up-regulation of NRP2 in more aggressive BrCa and HNSCC cell lines (**fig. 1A-D**). In addition, previous data from our group has previously shown that NRP2 expression correlates with worse prognosis in BrCa patients[17]. Analysis of a cohort of 2765 BrCa patients using the Kaplan-Meier plot database[26] showed that patients with high NRP2 expression have shorter distant metastasis free survival (DMFS) periods (61.2 months) than patients with low NRP2

expression (116 months) (**fig. 6A**). Similarly, higher levels of NRP2 in patients positively correlated with higher risk of developing metastasis and worse patients' DMFS in a cohort of 92 HNSCC patients, (**fig. 6B**). Therefore, these results reveal that NRP2 expression correlates with a higher risk of metastasis development, identifying it as a suitable biomarker candidate of metastatic risk.

DISCUSSION

Signalling crosstalk between sympathetic, parasympathetic, or sensory nerves and nervous system-related factors in the TME and tumour cells regulates cancer initiation, progression, or metastasis of diverse cancers, including pancreatic, gastric, colon, prostate breast, oral, and skin cancers, often through neurotransmitter, neuropeptides and axon guidance dependent signalling cascades[11,13,22,40,41]. Specifically, our data shows that NRP2 expression protects tumour cells from apoptosis and predisposes them to escape from dormancy and proliferate both in the primary tumour and in the context of lung metastasis. Moreover, our results strongly support that NRP2-dependent proliferation enhancement is mediated through the inhibition of the dormancy-associated transcription factor p27Kip1. In addition, we found that NRP2-dependent tumour-promoting effects in lung metastases require stromal TGFβ1, which is largely secreted by lung fibroblasts and macrophages.

Our results reveal a tumour promoting function for NRP2 both in basal BrCa and HNSCC (**fig. 1, 2**) by inhibiting tumour cells quiescence, promoting colony formation, and proliferation both *in vitro* and *in vivo*. In agreement with our results, NRP2 has been described to play a key role in tumour growth, regulating several tumorigenic processes such as cell proliferation[19]. In general, high levels of NRP2 have been associated with more proliferative breast[17], lung[42], melanoma[43], colorectal[44] and head and neck[45] tumours. However, the mechanisms by which NRP2 induces cell proliferation are not well understood.

Here we describe that NRP2 prevents cell cycle arrest through p27 down-modulation. In concordance with our data, in gastric cancer, NRP1 depletion downregulated Ki67 levels, induced p27 expression and cell cycle arrest[46], although the mechanisms underlying the NRPs regulation of p27 remain unknown. There might be other mechanisms underlying the link between NRP2 and proliferation. For instance in adipose-derived stem cells keratinocyte growth factor promotes Rb protein phosphorylation and inactivation through NRP1[47].

Our results show that NRP2 also promotes cancer cells invasion and dissemination (**fig. 3, 5**) which is in agreement with previous reports where they found that NRP2 regulates

endothelial and tumour cells migration[32,44,45]. Interestingly, our studies have revealed for the first time that lung DTCs over-express NRP2, and that its expression is required to drive cancer cell proliferation to form metastases (**fig. 3**). These data suggest that the lung microenvironment may selectively regulate NRP2 expression in DTCs. Consistently, recent papers in lung cancer have demonstrated that the lung microenvironment positively regulates NRP2 but no NRP1 expression[42]. Among known NRP2 regulators, we found NRP2 overexpression elicited selectively by TGFβ1 but not VEGF-C or SEMF3F. Moreover, this overexpression was partially abrogated by an inhibitor of the canonical TGFβ1 pathway, implicating TGF-β receptor activation of SMAD2/SMAD3 in this process. Consistently, Nasarre *et al* showed that NRP2 was up-regulated by TGFβ1[42] and a recent study has shown that SMAD3 increases NRP2 expression by binding to its mRNA 5' untranslated region[48]. In addition, genetic or chemical inhibition of SMAD4 also decreased NRP2 levels impairing tumour cell migration[44]. Conversely, NRP2 up-regulation has also been described as a SMAD independent process where ERK and AKT signalling pathways could be involved[42,45]. In our model, we found that NRP2 upregulation was partly reverted by TGFβ receptor I or by TGFβ I depletion suggesting that NRP2 regulation in lung DTCs is partly dependent on TGFβ1 canonical pathway.

Our results indicate that lung fibroblasts and macrophages derived TGFβ1 induces NRP2 expression. Inhibition or ablation of lung macrophages reduced BrCa metastases burden[49], even when metastases were already established[50], confirming the requirement of macrophages for lung metastatic seeding and growth. This agrees with our results that show that macrophages production of TGFβ1 up-regulates NRP2 expression in lung DTCs, promoting DTCs reprograming from dormancy to proliferation and progression to metastasis growth. It has also been shown that the composition of the stroma determines the fate of DTCs where type I and III collagen and fibronectin induced the proliferation of dormant BrCa DTCs developing proliferative lung metastatic lesions[39,51,52]. The most abundant factor secreted by activated fibroblasts is TGFβ1[53]. In accordance, we have found that CCD19-LU lung fibroblasts synthetized and secreted TGFβ1 to the media. TGFβ1 has already been shown to promote dormant BrCa DTCs re-awakening[7,8,39]. Here, we have additionally shown that old and fibrotic lung-derived TGFβ1 up-regulates NRP2 expression suggesting that NRP2 might have a crucial role in cell quiescence inhibition and proliferation activation in fibrotic lungs. In agreement with this, Fane et al., has recently shown that the aged lung microenvironment facilitates the outgrowth of dormant melanoma DTCs[54]. Although the detailed mechanisms are undefined, previous work suggest that Wnt pathway may be implicated, since in TGFβ1-mediated fibrosis the canonical Wnt pathway is activated, which in turn stimulates fibroblasts differentiation

and activation[55] and blocking canonical Wnt signalling down-regulated NRP2 expression[56] and resulted in a suppression of tumour growth and lung metastasis[57].

Finally, our results unveil that NRP2 expression correlates with worse prognosis and with a higher risk of developing metastases in both breast and head and neck cancer. This is in agreement with a recent report from Kang *et al.*, where they also showed that high expression of NRP2 correlated with lymph node metastasis and distant metastasis in oesophageal squamous cell carcinoma (OSCC) patients[58] and with our previous data where we showed that high expression of SEMA3F and NRP2 correlated with occult lymph node metastasis in HNSSC[18] and that high expression of NRP2 associates with worse prognosis in BrCa[17]. In fact, knocking out NRP2 expression, decreased micro-metastases size, and more interestingly, reprogramed single DTCs to quiescence both in HNSCC and BrCa models (**fig. 5**). Some reports have previously suggested a role of NRP2 in cancer metastasis[59]. For instance, NRP2 was shown to promote metastasis in OSCC through deregulation of ERK-MAPK-ETV4-MMP-E-cadherin pathway[45]. In another study, NRP2 interaction with integrin-β1 promoted FAK/ERK/HIF-1α/VEGF signalling favouring metastasis[60]. In BrCa, inhibition of NRP2 using a blocking antibody, was shown to prevent tumour lymphangiogenesis and metastasis, in part by modulating VEGFR3 signalling[59]. In our study, NRP2 seems to protect lung DTCs from apoptosis and promote lung metastasis formation through p27 inhibition, which triggers DTCs escape from dormancy and its switch into a proliferative behaviour. Overall, our results show that stromal TGFβ1 induces NRP2 expression that protects lung DTCs from apoptosis and induces the reprogramming of lung DTCs into a proliferative phenotype, increasing lung metastases development. Our findings have potential clinical implications and may lead to the use of NRP2 as a biomarker to predict tumour recurrences, as well as a therapeutic intervention target to reduce metastasis dissemination and outgrowth through NRP2 inhibition.

FIGURES

Figure 1

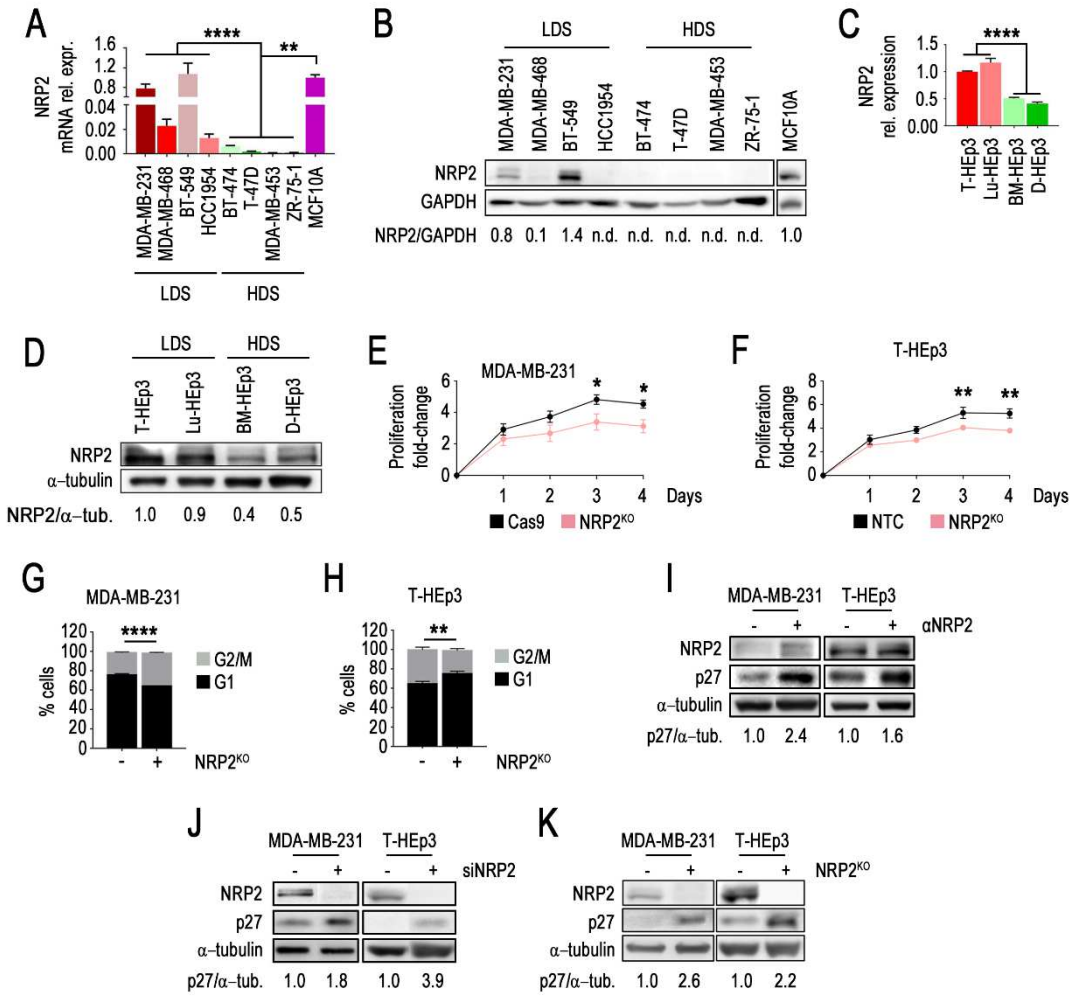

Figure 1. NRP2 deletion in proliferative cells alters cell cycle and decreases cell proliferation, by inducing p27 expression. A) Analysis of *NRP2* mRNA relative expression in human healthy mammary epithelial (MCF10A) and BrCa cell lines. The bar plot shows relative quantification (RQ) values referred to MCF10A cells (n=3). The graph represents RQ mean values ± S.E.M.; **P < 0.01, ****P < 0.0001 comparing LDS (MDA-MB-231, MDA-MB-468, HCC1954, BT-549) *vs* HDS (BT-474, T-47D, MDA-MB-453, ZR-75-1) cell lines by *t*-Student's test. **B)** Representative western blot analysis of NRP2 protein levels normalized with GAPDH. Protein quantifications are referred to MCF10A. n.d.=non detectable. (n=3). **C)** Analysis of *NRP2* mRNA relative expression in HNSCC cell lines. The bar plot shows RQ mean values ± S.E.M. referred to T-HEp3 cells (n=3); ****P < 0.0001 comparing proliferative/LDS (T-HEp3, Lu-HEp3) *vs* dormant/HDS (BM-HEp3, D-HEp3) cell lines by *t*-Student's test. **D)** Representative western blot analysis of NRP2 protein levels normalized with α-tubulin. Protein quantifications are referred to T-HEp3 cells (n=3). **E, F)** MDA-MB-231 (**E**) and T-HEp3 (**F**) cells proliferation in control (Cas9, NTC) *vs NRP2*-deleted cells ($NRP2^{KO}$). Graphs represent the fold-change of proliferation mean ±

S.E.M. referred to day 0 (n=2); *P < 0.05, **P < 0.01 comparing Cas9/NTC *vs* NRP2^{KO} by one-way ANOVA, Sidak's test. **G, H)** Percentage (%) of MDA-MB-231 (**G**) and T-HEp3 cells (**H**) in each cell cycle's phase in control (-) and *NRP2*-deleted (NRP2^{KO}) cells (+). The bar plots represent mean ± S.E.M. (n≥2); **P < 0.01, ****P < 0.0001 comparing Cas9/NTC (non-targeted cells) *vs* NRP2^{KO} by two-way ANOVA, Sidak's test. **I, J, K)** Representative western blot analysis of NRP2 and p27 protein levels normalized with α-tubulin after treatment with αNRP2 (1µg/mL) (n=3) (**I**), siNRP2 (50nM) (n=3) (**J**) or in orNRP2^{KO} cells(n=3) (**K**). p27 quantifications are referred to the non-treated conditions.

Figure 2

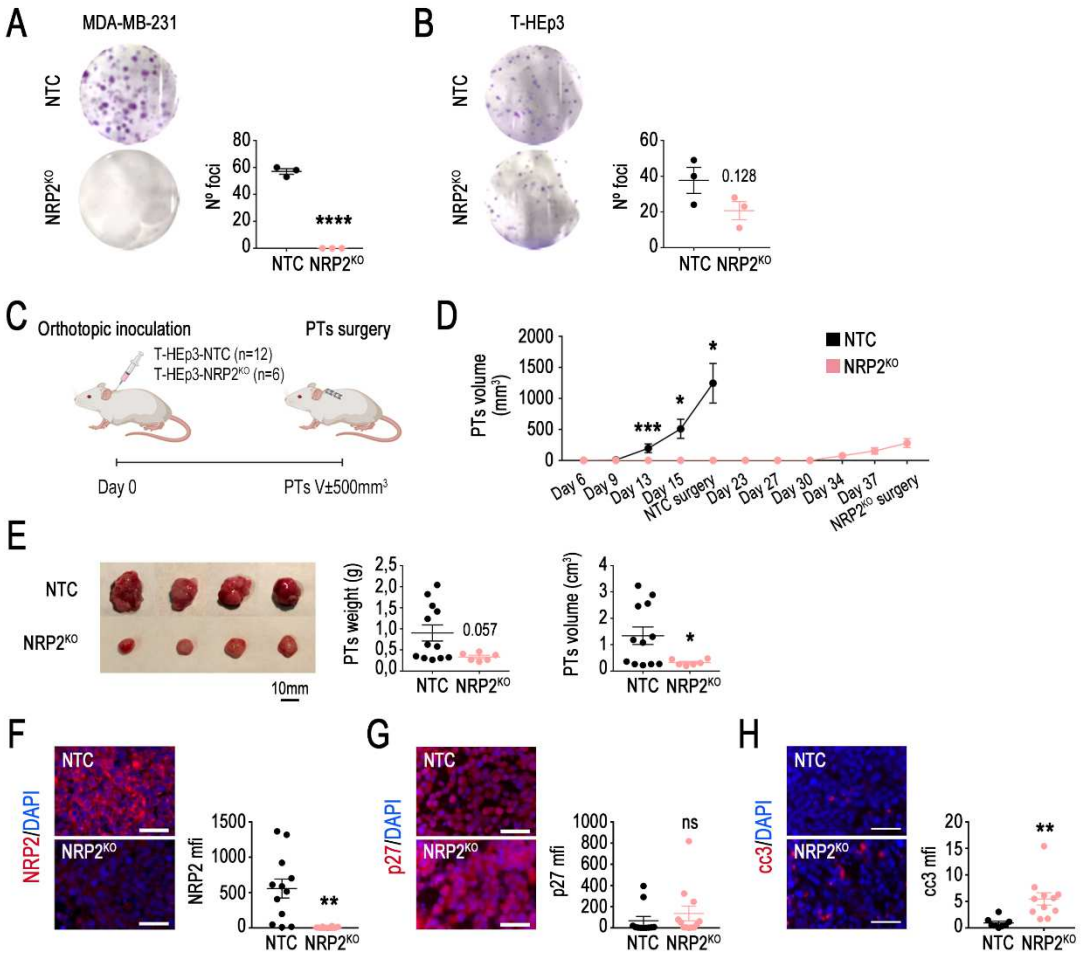

Figure 2. NRP2 deletion inhibits T-HEp3 tumour growth. A, B) Left panels, representative images of colonies from anchorage-dependent growth assay in MDA-MB-231 (**A**) and T-HEp3 (**B**) cells. Right graphs, quantification of the total number of colonies. Graphs represent mean ± S.E.M. (n=1, triplicates); ns, non-significant, ****P < 0.0001, comparing non-target control (NTC) *vs* NRP2^{KO} by *t*-Student's test. **C)** Diagram of the orthotopic mice *in vivo* experiment using T-HEp3 control (NTC) *vs NRP2*-depleted (NRP2^{KO}) cells. **D)** Graph representing T-HEp3 tumours volume (mm^3) over time for each group. **E)** Left panel, representative T-HEp3 tumour images at the time of surgery. Middle and right panels, graphs showing PTs weight (g) (middle) and volume (cm^3) (right) at the time of surgery. **F, G, H)** Left panels, representative immunofluorescence (IF) images of NRP2 (**F**), p27 (**G**) and cc3 (**H**) in T-HEp3 mice tumours. Scale bar: 50µm. Right panels, mean fluorescence intensity (mfi) quantification of NRP2, p27 and cc3. Graphs represent mean ± S.E.M. (n=1, with 12 mice for NTC and 6 mice for NRP2^{KO}); *P < 0.05, **P < 0.01, ***P < 0.001 comparing NTC *vs* NRP2^{KO} by *t*-Student's test.

Figure 3

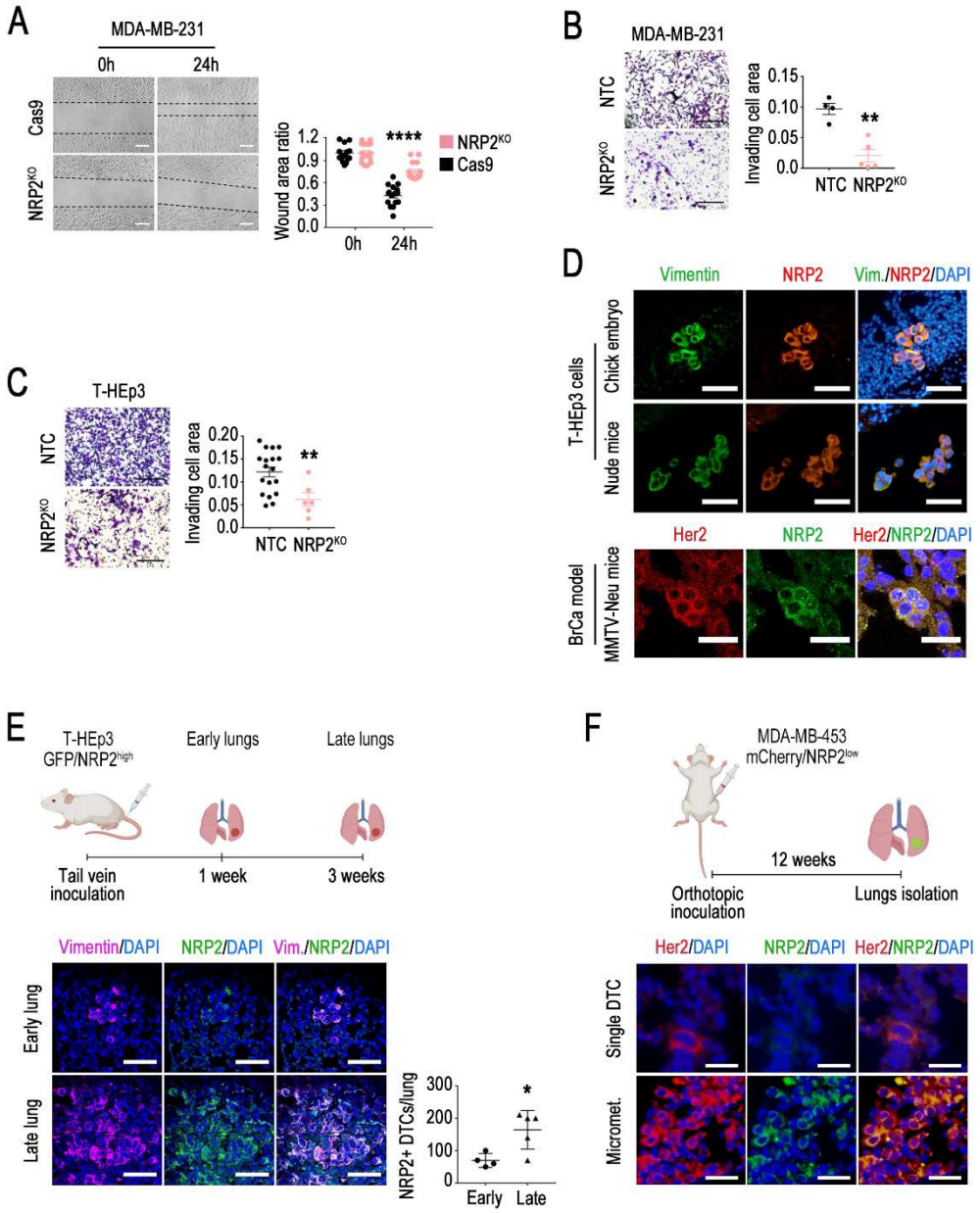

Figure 3. NRP2 induces cell motility and its expression is up-regulated in lung DTCs and lung metastases *in vivo*. A) Wound healing assay in MDA-MB-231 cells. Left panel, representative images from phase-contrast microscopy. Right panel, quantification of the wound area ratio after 0 and 24h migration in control (Cas9) and NRP2^{KO} MDA-MB-231 cells. Scale bar: 150µm. Graphs represent mean ± S.E.M. (n≥2); ****P < 0.0001, comparing Cas9 *vs* NRP2^{KO} by two-way ANOVA, Sidak's test. **B, C)** Invasion assay in MDA-MB-231 (**B**) and T-HEp3 (**C**) cells. Left panels, representative images from phase-contrast microscopy. Scale bar: 200µm. Right panels, quantification of the invading cells area. Graphs represent mean ± S.E.M. (n=2); **P < 0.01 comparing Cas9/NTC *vs* NRP2^{KO} by *t*-Student's test. **D)** Top and middle panels, representative IF images of vimentin (green) and NRP2 (red) staining of lung T-HEp3 DTCs in

chick embryo (top; scale bar: 50μm) and mice (middle; scale bar: 50μm) lung sections. Bottom panel, representative IF images of NRP2 (green) and HER2 (red) staining in MMTV-Neu mice lung sections. Scale bar: 20μm. **E)** Upper panel, diagram of the tail vein *in vivo* injection using T-HEp3 cells. Lower panel, representative IF images of vimentin (pink) and NRP2 (green) in T-HEp3 lung DTCs from early (isolated 1 week post-inoculation) and late (isolated 3 weeks post-inoculation) mice tail vein injection *in vivo* models. Scale bar: 50μm. The graph represents the number of NRP2-positive lung DTCs mean ± S.E.M.; *P < 0.05 comparing early vs late by *t*-Student's test. **F)** Upper panel, diagram of the orthotopic mice *in vivo* experiment using MDA-MB-453 mCherry+ cells. Lower panel, representative IF images of HER2 (red) and NRP2 (green) staining in lung MDA-MB-453 single DTCs and micrometastases (micromets). Scale bar: 50μm.

Figure 4

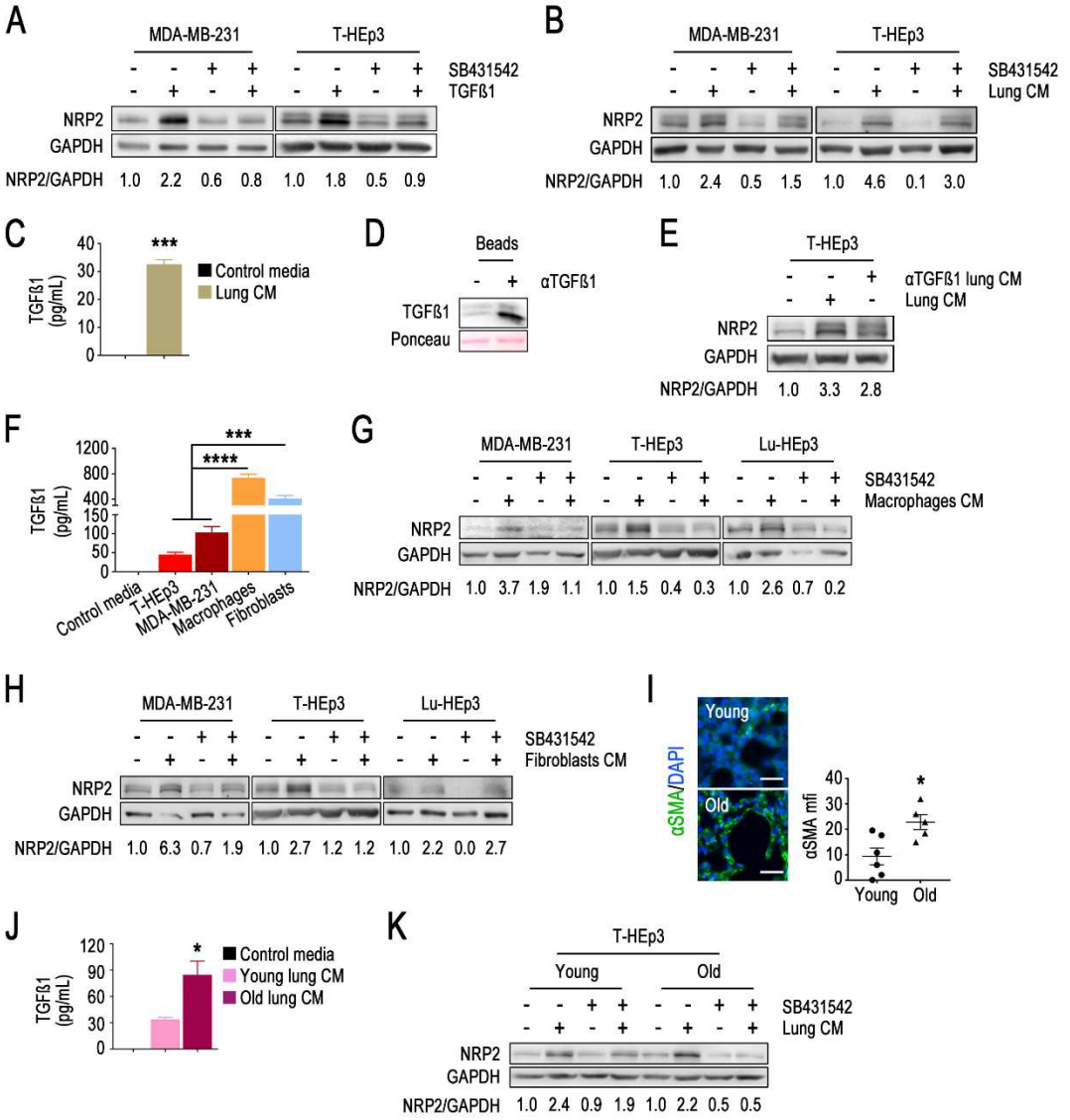

Figure 4. Lung fibroblasts and macrophages-derived TGFβ1 drives NRP2 up-regulation. A) Representative western blot analysis of NRP2 protein levels normalized with GAPDH after 24h treatment with SB431542 (5μM) and/or TGFβ1 (5ng/mL) (n=3). **B)** Representative western blot analysis of NRP2 protein levels normalized with GAPDH after 24h treatment with lung CM and/or SB431542 (5μM) (n=2). **C)** Quantification of TGFβ1 levels by ELISA (pg/mL) in lung CM. The graph represents the TGFβ1 pg/mL mean values ± S.E.M (n=1, triplicates); ***P < 0.001 comparing control media *vs* lung CM by *t*-Student's test. **D)** Representative western blot analysis of TGFβ1 protein levels released from the beads used for lung CM depletion used in **E**. Beads (-) refers to the control condition where control IgG-bound beads have been used for the assay whereas beads (+) refers to those beads linked to TGFβ1 antibody. **E)** Representative western blot analysis of NRP2 protein levels normalized with GAPDH after 24h treatment with lung CM or TGFβ1-depleted lung CM (n=1). **F)** Quantification of TGFβ1 levels by ELISA (pg/mL) in tumour cells (T-HEp3, MDA-MB-231) and TME cells (macrophages, THP-1; fibroblasts, CCD19)

conditioned media. The graph represents the TGFβ1 pg/mL mean values ± S.E.M (n=1, triplicates); ***P < 0.001, ****P < 0.0001 comparing tumour cells (T-HEp3 and 231) *vs* THP-1 or CCD19 by one-way ANOVA, Sidak's test. **G, H)** Representative western blot analysis of NRP2 protein levels normalized with GAPDH after 24h treatment with macrophages (THP-1) CM and SB431542 (5μM) (**G**) or fibroblasts (CCD19) CM and SB431542 (5μM) (**H**) (n=2). **I)** Left panel, representative IF images of αSMA in young and old mouse lungs (scale bar: 3μm). Right panels, αSMA mfi quantifications. **J)** TGFβ1 quantification by ELISA (pg/mL) in young and old mouse lung CM (n=1, triplicates). Graphs represent mean ± S.E.M.; *P < 0.05 comparing young *vs* old by one-way ANOVA, Sidak's test. **K)** Representative western blot analysis of NRP2 protein levels normalized with GAPDH after 24h treatment with young or old mouse lung CM and SB431542 (5μM) (n=1). In all the western blots, NRP2 protein quantifications are referred to the non-treated control conditions.

Figure 5

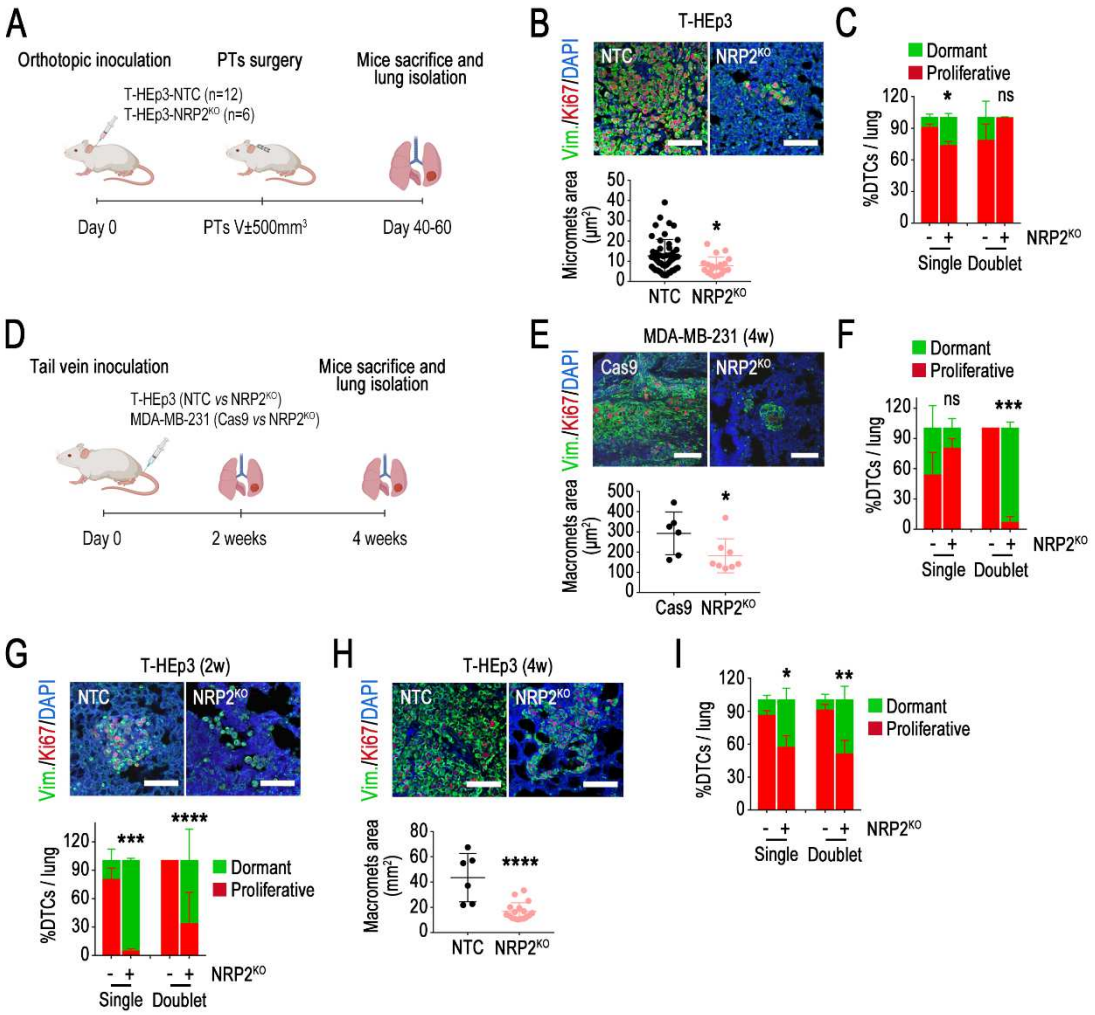

Figure 5. NRP2 deletion decreases lung metastases size and triggers quiescence in lung DTCs *in vivo*. A) Diagram of the orthotopic mice *in vivo* injection using T-HEp3 cells. **B)** Upper panel, representative IF images of vimentin (Vim.; green) and Ki67 (red) staining of T-HEp3 lung DTCs (scale bar: 100µm). Lower panel, quantification of lung micrometastases area (µm^2) using ImageJ software. **C)** Quantification of the percentage (%) of Ki67-positive (proliferative) or Ki67-negative (dormant) single and doublet T-HEp3 cells per lung. **D)** Diagram of the tail vein mice *in vivo* injection using MDA-MB-231 or T-HEp3 cells. **E)** Upper panel, representative IF images of vimentin (Vim.; green) and Ki67 (red) staining of MDA-MB-231 lung DTCs 4 weeks (4w) after inoculation (scale bar: 50µm). Lower panel, quantification of lung macrometastases area (µm^2) using ImageJ software. **F)** Quantification of the % of Ki67-positive or Ki67-negative single and doublet MDA-MB-231 cells per lung. **G)** Upper panel, representative IF images of vimentin (Vim.; green) and Ki67 (red) staining of T-HEp3 lung DTCs 2 weeks (2w) after inoculation (scale bar: 50µm). Lower panel, quantification of the % of Ki67-positive or Ki67-negative single and doublet T-HEp3 cells per lung. **H)** Upper panel, representative IF images of vimentin (Vim.; green) and Ki67 (red) staining of T-HEp3 lung DTCs 4 weeks (4w) after inoculation (scale bar: 50µm). Lower

panel, quantification of lung macrometastases area (mm^2) using ImageJ software. **I)** Quantification of the % of Ki67-positive or Ki67-negative single and doublet T-HEp3 cells per lung. Graphs represent mean ± S.E.M. (n≥5 lungs per group); ns, non-significant, *P < 0.05, **P < 0.01, ***P < 0.001, ****P < 0.0001 comparing NTC *vs* $NRP2^{KO}$ by *t*-Student's test.

Figure 6

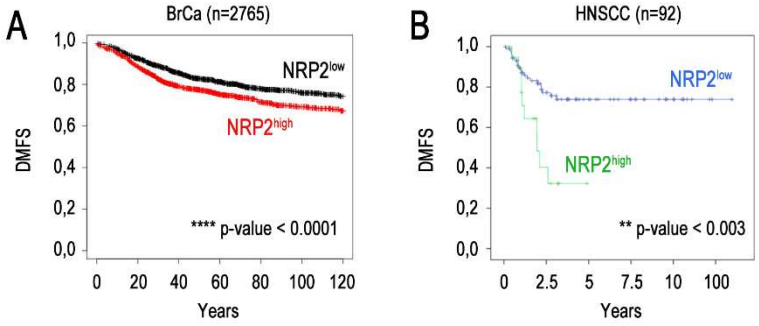

Figure 6. High levels of NRP2 negatively correlate with BrCa and HNSCC patients' DMFS. A) Kaplan-Meier curve for distant metastases-free survival (DMFS) in a cohort of 2765 BrCa patients with high (red; n=1437) or low (black; n=1328) levels of NRP2. Adapted from Győrffy *et al*. [1]. **B)** Kaplan-Meier curve for DMFS in a cohort of 92 HNSCC patients with high (green; n=20) or low (blue; n=72) levels of NRP2. Analysis performed in collaboration with Dr. Camacho and Dr. Leon from Santa Creu I Sant Pau Hospital (Barcelona, Spain).

REFERENCES

1 Welch, D. R. & Hurst, D. R. Defining the Hallmarks of Metastasis. *Cancer Res* **79**, 3011-3027, doi:10.1158/0008-5472.CAN-19-0458 (2019).

2 Sosa, M. S., Bragado, P. & Aguirre-Ghiso, J. A. Mechanisms of disseminated cancer cell dormancy: an awakening field. *Nat Rev Cancer* **14**, 611-622, doi:10.1038/nrc3793 (2014).

3 Aguirre-Ghiso, J. A. Models, mechanisms and clinical evidence for cancer dormancy. *Nat Rev Cancer* **7**, 834-846, doi:10.1038/nrc2256 (2007).

4 Gomis, R. R. & Gawrzak, S. Tumor cell dormancy. *Mol Oncol* **11**, 62-78, doi:10.1016/j.molonc.2016.09.009 (2017).

5 Mathot, L. & Stenninger, J. Behavior of seeds and soil in the mechanism of metastasis: a deeper understanding. *Cancer Sci* **103**, 626-631, doi:10.1111/j.1349-7006.2011.02195.x (2012).

6 Paget, S. The distribution of secondary growths in cancer of the breast. 1889. *Cancer Metastasis Rev* **8**, 98-101 (1989).

7 Bragado, P. *et al.* TGF-beta2 dictates disseminated tumour cell fate in target organs through TGF-beta-RIII and p38alpha/beta signalling. *Nat Cell Biol* **15**, 1351-1361, doi:10.1038/ncb2861 (2013).

8 Ghajar, C. M. *et al.* The perivascular niche regulates breast tumour dormancy. *Nat Cell Biol* **15**, 807-817, doi:10.1038/ncb2767 (2013).

9 Yumoto, K. *et al.* Axl is required for TGF-beta2-induced dormancy of prostate cancer cells in the bone marrow. *Sci Rep* **6**, 36520, doi:10.1038/srep36520 (2016).

10 Kobayashi, A. *et al.* Bone morphogenetic protein 7 in dormancy and metastasis of prostate cancer stem-like cells in bone. *J Exp Med* **208**, 2641-2655, doi:10.1084/jem.20110840 (2011).

11 Mancino, M., Ametller, E., Gascon, P. & Almendro, V. The neuronal influence on tumor progression. *Biochim Biophys Acta* **1816**, 105-118, doi:10.1016/j.bbcan.2011.04.005 (2011).

12 Cole, S. W., Nagaraja, A. S., Lutgendorf, S. K., Green, P. A. & Sood, A. K. Sympathetic nervous system regulation of the tumour microenvironment. *Nat Rev Cancer* **15**, 563-572, doi:10.1038/nrc3978 (2015).

13 Magnon, C. *et al.* Autonomic nerve development contributes to prostate cancer progression. *Science* **341**, 1236361, doi:10.1126/science.1236361 (2013).

14 Zhao, C. M. *et al.* Denervation suppresses gastric tumorigenesis. *Sci Transl Med* **6**, 250ra115, doi:10.1126/scitranslmed.3009569 (2014).

15 Pascual, G. *et al.* Dietary palmitic acid promotes a prometastatic memory via Schwann cells. *Nature* **599**, 485-490, doi:10.1038/s41586-021-04075-0 (2021).

16 Decker, A. M. *et al.* Sympathetic Signaling Reactivates Quiescent Disseminated Prostate Cancer Cells in the Bone Marrow. *Mol Cancer Res* **15**, 1644-1655, doi:10.1158/1541-7786.MCR-17-0132 (2017).

17 Fernandez-Nogueira, P. *et al.* Differential expression of neurogenes among breast cancer subtypes identifies high risk patients. *Oncotarget* **7**, 5313-5326, doi:10.18632/oncotarget.6543 (2016).

18 Meler-Claramonte, C. *et al.* Semaphorin-3F/Neuropilin-2 Transcriptional Expression as a Predictive Biomarker of Occult Lymph Node Metastases in HNSCC. *Cancers (Basel)* **14**, doi:10.3390/cancers14092259 (2022).

19 Prud'homme, G. J. & Glinka, Y. Neuropilins are multifunctional coreceptors involved in tumor initiation, growth, metastasis and immunity. *Oncotarget* **3**, 921-939, doi:10.18632/oncotarget.626 (2012).

20 Raimondi, C. & Ruhrberg, C. Neuropilin signalling in vessels, neurons and tumours. *Semin Cell Dev Biol* **24**, 172-178, doi:10.1016/j.semcdb.2013.01.001 (2013).

21 Fernandez-Nogueira, P. *et al.* Tumor-Associated Fibroblasts Promote HER2-Targeted Therapy Resistance through FGFR2 Activation. *Clin Cancer Res* **26**, 1432-1448, doi:10.1158/1078-0432.CCR-19-0353 (2020).

22 Zubeldia-Plazaola, A. *et al.* Glucocorticoids promote transition of ductal carcinoma in situ to invasive ductal carcinoma by inducing myoepithelial cell apoptosis. *Breast Cancer Res* **20**, 65, doi:10.1186/s13058-018-0977-z (2018).

23 Shalem, O. *et al.* Genome-scale CRISPR-Cas9 knockout screening in human cells. *Science* **343**, 84-87, doi:10.1126/science.1247005 (2014).

24 Harper, K. L. *et al.* Mechanism of early dissemination and metastasis in Her2(+) mammary cancer. *Nature* **540**, 588-592, doi:10.1038/nature20609 (2016).

25 Ringner, M., Fredlund, E., Hakkinen, J., Borg, A. & Staaf, J. GOBO: gene expression-based outcome for breast cancer online. *PLoS One* **6**, e17911, doi:10.1371/journal.pone.0017911 (2011).

26 Nagy, A., Munkacsy, G. & Gyorffy, B. Pancancer survival analysis of cancer hallmark genes. *Sci Rep* **11**, 6047, doi:10.1038/s41598-021-84787-5 (2021).

27 Kim, R. S. *et al.* Dormancy signatures and metastasis in estrogen receptor positive and negative breast cancer. *PLoS One* **7**, e35569, doi:10.1371/journal.pone.0035569 (2012).

28 Adam, A. P. *et al.* Computational identification of a p38SAPK-regulated transcription factor network required for tumor cell quiescence. *Cancer Res* **69**, 5664-5672, doi:10.1158/0008-5472.CAN-08-3820 (2009).

29 Coqueret, O. New roles for p21 and p27 cell-cycle inhibitors: a function for each cell compartment? *Trends Cell Biol* **13**, 65-70, doi:10.1016/s0962-8924(02)00043-0 (2003).

30 Aguirre-Ghiso, J. A., Estrada, Y., Liu, D. & Ossowski, L. ERK(MAPK) activity as a determinant of tumor growth and dormancy; regulation by p38(SAPK). *Cancer Res* **63**, 1684-1695 (2003).

31 Fantozzi, A. & Christofori, G. Mouse models of breast cancer metastasis. *Breast Cancer Res* **8**, 212, doi:10.1186/bcr1530 (2006).

32 Alghamdi, A. A. A. *et al.* NRP2 as an Emerging Angiogenic Player; Promoting Endothelial Cell Adhesion and Migration by Regulating Recycling of alpha5 Integrin. *Front Cell Dev Biol* **8**, 395, doi:10.3389/fcell.2020.00395 (2020).

33 Wittmann, P. *et al.* Neuropilin-2 induced by transforming growth factor-beta augments migration of hepatocellular carcinoma cells. *BMC Cancer* **15**, 909, doi:10.1186/s12885-015-1919-0 (2015).

34 Wang, J. *et al.* NRP-2 in tumor lymphangiogenesis and lymphatic metastasis. *Cancer Lett* **418**, 176-184, doi:10.1016/j.canlet.2018.01.040 (2018).

35 Giger, R. J. *et al.* Neuropilin-2 is required in vivo for selective axon guidance responses to secreted semaphorins. *Neuron* **25**, 29-41, doi:10.1016/s0896-6273(00)80869-7 (2000).

36 Nasarre, P., Gemmill, R. M. & Drabkin, H. A. The emerging role of class-3 semaphorins and their neuropilin receptors in oncology. *Onco Targets Ther* **7**, 1663-1687, doi:10.2147/OTT.S37744 (2014).

37 Casanova-Acebes, M. *et al.* Tissue-resident macrophages provide a pro-tumorigenic niche to early NSCLC cells. *Nature* **595**, 578-584, doi:10.1038/s41586-021-03651-8 (2021).

38 Ikemori, R. *et al.* Epigenetic SMAD3 Repression in Tumor-Associated Fibroblasts Impairs Fibrosis and Response to the Antifibrotic Drug Nintedanib in Lung Squamous Cell Carcinoma. *Cancer Res* **80**, 276-290, doi:10.1158/0008-5472.CAN-19-0637 (2020).

39 Barkan, D. *et al.* Metastatic growth from dormant cells induced by a col-I-enriched fibrotic environment. *Cancer Res* **70**, 5706-5716, doi:10.1158/0008-5472.CAN-09-2356 (2010).

40 Zahalka, A. H. & Frenette, P. S. Nerves in cancer. *Nat Rev Cancer* **20**, 143-157, doi:10.1038/s41568-019-0237-2 (2020).

41 Fernandez-Nogueira, P. *et al.* Histamine receptor 1 inhibition enhances antitumor therapeutic responses through extracellular signal-regulated kinase (ERK) activation in breast cancer. *Cancer Lett* **424**, 70-83, doi:10.1016/j.canlet.2018.03.014 (2018).

42 Nasarre, P. *et al.* Neuropilin-2 Is upregulated in lung cancer cells during TGF-beta1-induced epithelial-mesenchymal transition. *Cancer Res* **73**, 7111-7121, doi:10.1158/0008-5472.CAN-13-1755 (2013).

43 Moriarty, W. F., Kim, E., Gerber, S. A., Hammers, H. & Alani, R. M. Neuropilin-2 promotes melanoma growth and progression in vivo. *Melanoma Res* **26**, 321-328, doi:10.1097/CMR.0000000000000190 (2016).

44 Grandclement, C. *et al.* Neuropilin-2 expression promotes TGF-beta1-mediated epithelial to mesenchymal transition in colorectal cancer cells. *PLoS One* **6**, e20444, doi:10.1371/journal.pone.0020444 (2011).

45 Fung, T. M. *et al.* Neuropilin-2 promotes tumourigenicity and metastasis in oesophageal squamous cell carcinoma through ERK-MAPK-ETV4-MMP-E-cadherin deregulation. *J Pathol* **239**, 309-319, doi:10.1002/path.4728 (2016).

46 Li, L. *et al.* Neuropilin-1 is associated with clinicopathology of gastric cancer and contributes to cell proliferation and migration as multifunctional co-receptors. *J Exp Clin Cancer Res* **35**, 16, doi:10.1186/s13046-016-0291-5 (2016).

47 Ceccarelli, S. *et al.* Neuropilin 1 Mediates Keratinocyte Growth Factor Signaling in Adipose-Derived Stem Cells: Potential Involvement in Adipogenesis. *Stem Cells Int* **2018**, 1075156, doi:10.1155/2018/1075156 (2018).

48 Xie, X. *et al.* Smad3 Regulates Neuropilin 2 Transcription by Binding to its 5' Untranslated Region. *J Am Heart Assoc* **9**, e015487, doi:10.1161/JAHA.119.015487 (2020).

49 Kitamura, T. *et al.* CCL2-induced chemokine cascade promotes breast cancer metastasis by enhancing retention of metastasis-associated macrophages. *J Exp Med* **212**, 1043-1059, doi:10.1084/jem.20141836 (2015).

50 Qian, B. *et al.* A distinct macrophage population mediates metastatic breast cancer cell extravasation, establishment and growth. *PLoS One* **4**, e6562, doi:10.1371/journal.pone.0006562 (2009).

51 Barney, L. E. *et al.* Tumor cell-organized fibronectin maintenance of a dormant breast cancer population. *Sci Adv* **6**, eaaz4157, doi:10.1126/sciadv.aaz4157 (2020).

52 Di Martino, J. S. *et al.* A tumor-derived type III collagen-rich ECM niche regulates tumor cell dormancy. *Nat Cancer* **3**, 90-107, doi:10.1038/s43018-021-00291-9 (2022).

53 Dai, L. *et al.* Fibroblasts in cancer dormancy: foe or friend? *Cancer Cell Int* **21**, 184, doi:10.1186/s12935-021-01883-2 (2021).

54 Fane, M. E. *et al.* Stromal changes in the aged lung induce an emergence from melanoma dormancy. *Nature* **606**, 396-405, doi:10.1038/s41586-022-04774-2 (2022).

55 Akhmetshina, A. *et al.* Activation of canonical Wnt signalling is required for TGF-beta-mediated fibrosis. *Nat Commun* **3**, 735, doi:10.1038/ncomms1734 (2012).

56 Ji, T. *et al.* Neuropilin-2 expression is inhibited by secreted Wnt antagonists and its down-regulation is associated with reduced tumor growth and metastasis in osteosarcoma. *Mol Cancer* **14**, 86, doi:10.1186/s12943-015-0359-4 (2015).

57 Jang, G. B. *et al.* Blockade of Wnt/beta-catenin signaling suppresses breast cancer metastasis by inhibiting CSC-like phenotype. *Sci Rep* **5**, 12465, doi:10.1038/srep12465 (2015).

58 Kang, Y., Zhang, Y., Zhang, Y. & Sun, Y. NRP2, a potential biomarker for oral squamous cell carcinoma. *Am J Transl Res* **13**, 8938-8951 (2021).

59 Caunt, M. *et al.* Blocking neuropilin-2 function inhibits tumor cell metastasis. *Cancer Cell* **13**, 331-342, doi:10.1016/j.ccr.2008.01.029 (2008).

60 Lv, T. *et al.* p53-R273H upregulates neuropilin-2 to promote cell mobility and tumor metastasis. *Cell Death Dis* **8**, e2995, doi:10.1038/cddis.2017.376 (2017).

ACKNOWLEDGEMENTS: The authors thank Darya Kulyk for her help preparing the schemes that are shown in the figures. This work was supported by grants from the Spanish Ministry of Economy and Competitiveness [PID2019-104991RB-I00 to P.B., PID2019-104143RB-C22 to A.P.]. All funding was cosponsored by the European FEDER Program. L.R-P. and S.M. were recipients of FPU fellowships from Spanish Ministry of Education. A.G-U. and M.R. are supported by Madrid Community Program for Talent Attraction (2017-T1/BMD-5468). P.F.-N. is supported by a Juan de la Cierva contract from the Spanish Ministry of science, innovation and universities. P.F.-N. and G.F. are supported by Cellex Foundation. P.F.-N., G.F., N.C. and P.G. are funded by La Marató TV3 (201915-30-31), and by Secretaria d'Universitats i Recerca del Departament d'Economia i Coneixement (2017_SGR_1305). P.B. received support from BBVA (Becas Leonardo 2018, BBM-TRA-0041). J.A.A-G was supported by The National Institute of Health /National Cancer Institute (Grant CA109182) and the Samuel Waxman Cancer Research Foundation Tumor Dormancy Program. E.D. was funded by The National Institute of Health /National Cancer Institute (T32 CA078207).

AUTHOR CONTRIBUTIONS: L.R-P. (first author) contributed to design the experiments, performed most of the experiments, data analysis, data interpretation, draft and revised the paper. P.J., A.L-P., P.F-N., M.I-G., S.M., R.A., A.N-C., N.M., C.B., M.R., N.P. and E.D., performed some experiments, developed methodology and analysed data. F.X. A-J., I.V., X.L-V., M.C., G.F., J.A., J.A-G., P.G., A.G-U., A.P. and N.C. provided animals, acquired and managed patients samples, provided facilities, assist with the analysis and interpretation of data. P.B. designed most of the experiments, supervised all the work and wrote the manuscript. All the authors revised the manuscript.

COMPETING INTERESTS: JAAG is a scientific co-founder of scientific advisory board member and equity owner in HiberCell and receives financial compensation as a consultant for HiberCell, a Mount Sinai spin-off company focused on the research and development of therapeutics that prevent or delay the recurrence of cancer.

MATERIALS & CORRESPONDENCE.: Paloma Bragado (pbragado@ucm.es)

Supplementary Files

This is a list of supplementary files associated with this preprint. Click to download.

- Supplementarymaterial20220812.pdf